The 15th International Conference on Advanced Robotics
Tallinn University of Technology
Tallinn, Estonia, June 20-23, 2011

Simulation of Dynamics and Realistic Contact Forces for Manipulators and Legged Robots with High Joint Elasticity

Thomas Lens and Katayon Radkhah and Oskar von Stryk

Abstract— **In this paper, multibody system dynamics simulation for manipulators and legged robots with high joint elasticities, particularly with focus on collision modeling, is addressed. We present the architecture of a newly developed toolbox in conjunction with a detailed discussion of a realistic contact, friction and stiction model, which is validated with real measurement data of a bouncing ball. The work presented is driven and inspired by two concrete robot developments in the authors' group: the manipulator BioRob and the biped BioBiped. The libraries are used to develop kinematic and kinetic models of these bio-inspired and highly elastic robots. Models and simulation of both robots are discussed, as well as occurring forces during collisions of the BioRob-X4 arm with the ground. We are also able to demonstrate good agreement of ground contact forces measured during slow jogging motion of a human subject with simulation results obtained with BioBiped1.**

I. INTRODUCTION

A. Background

Multibody system (MBS) dynamics simulation is well-suited for realistic modeling of the time-dependent behavior of manipulators and legged robots as well as the effect of collisions with the environment. With respect to MBS dynamics simulation, an overwhelming wealth of research can be identified in the robotics and computer graphics community.

The equations and physics behind the simulation have been presented in several papers and are considered as generally accepted. For efficient calculations of inverse and forward dynamics of a rigid-body model of a robotic mechanism, a number of algorithms have been proposed [1]–[7].

Present software packages offer different capabilities in a variety of ways such as: computational speed, kinematic structures and joint models supported, level of detail, underlying robot dynamics formulation and associated order of complexity, user interface, graphics support, numerical integration routines, integration with other code, application support [8]. Among those often cited are: Adams, DynaMechs, Open Dynamics Engine (ODE) [9], Microsoft Robotics Studio, Webots. Given the standard or modified Denavit-Hartenberg (DH) parameters [10], the Robotics toolbox [11] can perform forward and inverse kinematics and dynamics by applying standard algorithms for serial link manipulators. Efficient symbolic and numeric calculation of kinematic and dynamic equations for multi-degree-of-freedom manipulators is enabled by Robotica [12]. SIMpact is a general framework for the dynamic simulation and haptic exploration of complex virtual environments involving analytical computation of contacts [13]–[15].

Many other toolboxes are designed for special purposes, for instance [16], [17] targeting at analysis, design and testing of control algorithms for robotic manipulators. OpenSim is a freely available, extensible software system that allows users to develop models of musculoskeletal structures and create dynamic simulations of movement.

In general, it can be stated, that often workarounds are necessary to compensate for missing features. Particularly the problem of visualization is often handled using, for instance, three-dimensional (3-D) animation software Maya or Blender in addition to a robot dynamics simulator.

B. Motivation

Efficient control strategies for manipulators and legged robots are based on sufficiently accurate and realistic contact modeling, as collisions with the environment are to be expected. In this regard many simulation software packages share the same deficiency. Either no, respectively a too simplifying [9], or a computationally expensive contact model is considered [18], [19]. Contact models have been researched for a while. But as far as we could ascertain, there is none (in the publicly available packages) that meets the requirements of a wide field of applications, such as manipulation tasks and legged locomotion, that also generates realistic impact, kinetic, and static friction forces, and finally integrates well into an existing simulation application without causing a blow-up in computational complexity. Furthermore, an increased use of active and passive mechanical elasticity in robotic systems can be observed. Elasticity is nowadays becoming generally accepted as an important property of manipulators for safe human-robot interaction and of legged robots for human-like movements. Both, contact modeling and elastic actuation, are of paramount importance in many recent robotic applications.

Within the authors' group two biologically inspired robots have been designed and developed: the robot arm BioRob [20], [21] (cf. Fig. 8(a)) and the bipedal robot BioBiped [22], [23] (cf. Fig. 9(a)). Intensified focus of these projects lies on safe human-robot interaction, operation of manipulators in human-like environments and the development of actuation and controllers for human-like locomotion. The investigation of the mentioned research topics requires, on the one hand, models of elastic actuators as well as of stiff actuators, to

Parts of this research have been supported by the German Research Foundation (DFG) under grant no. STR 533/7-1 and German Federal Ministry of Education and Research BMBF under grant 01 RB 0908 A.

All authors are members of the Simulation, Systems Optimization and Robotics Group, Technische Universität Darmstadt, Germany. E-mail: {lens,radkhah,stryk}@sim.tu-darmstadt.de

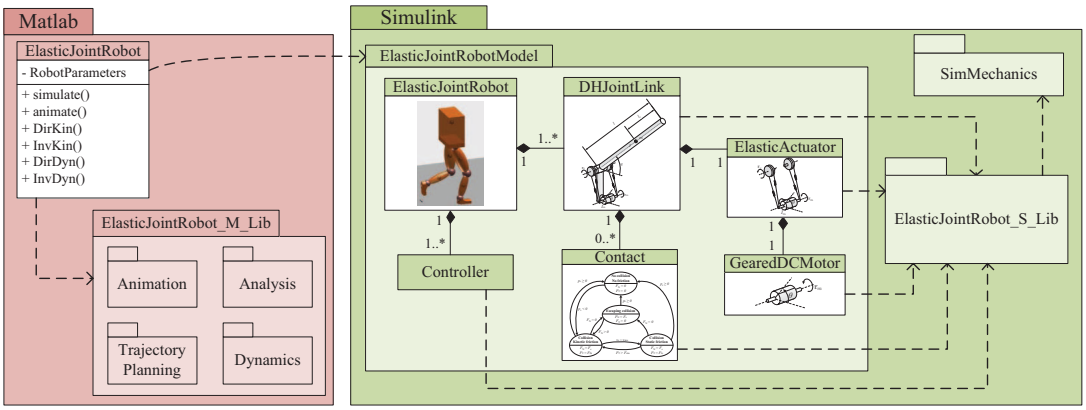

Fig. 1. Architecture of the developed toolbox including the Matlab and Simulink libaries for simulation of elastic joint robots.

provide the basis for comparisons, and a highly realistic contact model. On the other hand, the simulation environment should enable controller designs, the study of optimization problems, and a realistic animation.

All these features can hardly be found in one single software package. Therefore, the benefits of creating a tailored multibody simulation toolbox are evident. The solution developed by the authors is based on using the commercial off-the-shelf software tool Matlab [24] and Simulink [25] due to the ease of integration with other analysis, control and simulation programs. The proposed approach is feasible in any other technical computing environment as well. It should be also pointed out that the toolbox is intended to complement and not compete with existing packages more sophisticated for specific applications.

The decision criteria for Matlab include the use of object-oriented techniques. Besides, SimMechanics makes it easy to create a representation of a physical mechanism within a Simulink model. An important feature of SimMechanics embraces the generation of standalone code for faster simulation and deployment on rapid prototyping systems. Furthermore, with a large set of available well-established algorithms for solving equations of motion, numerical computation in Matlab is facilitated.

C. Outline of the Paper

Following this brief survey on existing simulation software packages and the discussion of the identified weaknesses, we give in Section 2 an overview of the developed toolbox architecture and its components. Here, particular focus lies on the clear presentation of the collision model. Section 3 addresses modeling and simulation of the MBS dynamics of the BioRob and BioBiped robots. A summary of the paper, highlighting benefits and limits of the proposed libraries, in conjunction with future directions is given in Section 4.

II. ARCHITECTURE OF THE SOFTWARE PACKAGE

The developed software consists of the Matlab and Simulink libaries, `ElasticJointRobot_M_Lib` and `ElasticJointRobot_S_Lib`, as depicted in (Fig. 1).

As the magnitude and complexity of MBS simulation tasks may rapidly increase, we chose an object-oriented design. In this way, designing and managing the data passed to functions do not become difficult and error prone. Data and operations are encapsulated in the objects.

The object ElasticJointRobot represents a robot and holds its parameters. The object provides methods to set trajectories and perform numerical computations such as kinematics and dynamics calculations. Some of its properties are initialized during model setup, others are set after numerical computations or simulation. The kinematics description is based on the standard DH convention. Other toolboxes such as [11] can therefore easily be combined and used.

For simulation of more complex dynamics, i. e., impact and friction behavior (cf. Section II-B), the object is coupled to a Simulink model. The model uses blocks from the Simulink library, `ElasticJointRobot_S_Lib`. This library holds blocks for modeling the mechanical structure of the robot (A), contacts (B), actuators (C), and, in addition, designing controllers (D). Animation (E) and analysis tools are part of the Matlab library, `ElasticJointRobot_M_Lib`.

A. Modular Joint-Link Structures

The concept of a multibody system can be understood as an abstract collection of bodies whose relative motions are constrained by means of joints and other more complicated constraints (springs, pulley systems, etc.). In general, it is possible to clearly identify combinations of different components that will appear more than once in a multibody system. Therefore, it is advisable to build ready combinations, and, in this way, making a complex model more manageable and understandable.

Among the ready combinations are blocks for rigid joint-link structures, that take either torques as input and compute the commonly required outputs (positions, velocities, accelerations) or take positions, velocities and accelerations as inputs and compute the inverse dynamics. Such blocks can also consider upper and lower joint boundaries. Further, a

dynamics model of a robot often needs blocks for representing the base or solely a rigid link.

B. Modeling Collisions/Contacts

Modeling dynamic contacts is a still quite challenging problem and, thus, a major contribution of this paper is the description of the newly developed contact model. A contact model should characterize both the forces that can be transmitted through the contact as well as the allowed relative motions of the contacting bodies. These characteristics are determined by the geometry of the contacting surfaces and the material properties of the parts which dictate friction and possible contact deformation.

We consider point contacts, because plane contacts can be treated as multiple point contacts at the corners of the contact area. A point contact is described as a state machine that switches between normal force, kinetic and static friction. It can be attached to any point of a body. Fig. 2(a) depicts the considered point contact model. For a realistic modeling of the dynamic properties, a finite surface A has to be assumed. L stands for the measured thickness of the contact layer. Collision forces, that are generated along the surface normal, are denoted as F_N. Tangential forces, that are caused by kinetic and static friction during a collision, are denoted as F_T.

Contact dynamics can be modeled by either penalty-based or analytical methods. Most analytical methods use optimization techniques to satisfy contact model conditions and produce relatively stable results even with large sampling time. However, optimization problems are often time-consuming and require simplification. In systems, where bouncing occurs more frequently than stick contacts, impulse-based methods are computationally more efficient than optimization problems. Based on the assumption of inelastic collisions, an iterative trial-and-error method is used in [26] to increase computational efficiency during stick contacts. Despite workarounds, a general disadvantage of analytical methods is that realistic impact and friction forces are difficult to predict. Also, it is possible that no solution or multiple solutions are found, and energy conservation principles may be violated in frictional impacts [27]. In contrast to analytical methods, penalty-based methods [28], [29] generate forces at the point contacts based on the elastic and viscous properties of the material. They incorporate deformations and losses of energy and can easily be enhanced by friction models. The coupling of the colliding objects with a virtual spring damper system possibly results in a stiff system of ordinary differential equations, which requires smaller simulation step sizes. This, however, is necessary anyway, when analyzing not only the motions, but also the impact and friction forces and their effect on the joint torques of the system.

In this section, we explain how to model contacts that are able to predict realistic contact forces including kinetic and static friction by using a state machine. In addition, we elucidate how the parameters of this model can be calculated from the material properties of the colliding bodies. Note, that this model can be used in any MBS dynamics simulation tool that allows to introduce forces into a body and measure the position and velocity of a body.

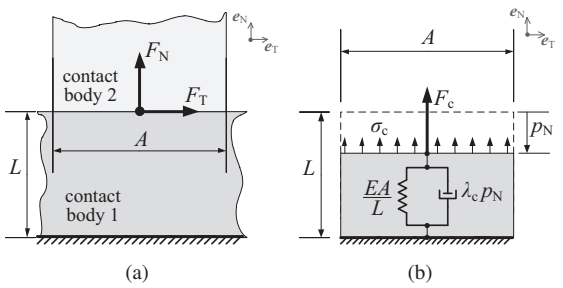

Fig. 2. Finite single point contact (a) and collision (b) model.

1) Collision: Fig. 2(a) displays two contacting bodies in a relaxed state and the normal and tangential forces, F_N and F_T, respectively. Fig. 2(b) illustrates the collision model. The collision counterforce F_c is computed depending on the penetration p_N along the surface normal vector $\boldsymbol{e}_N$. As mentioned earlier, the contact body 1 is assumed to have a smooth contact surface of size A with an infinite extension (ground, wall, etc.), so that a geometric collision detection can be reduced to:

$$p_\mathrm{N} = \boldsymbol{p} \cdot \boldsymbol{e}_\mathrm{N} \ , \tag{1}$$

where p_N is the relative distance between the colliding objects and negative during collision, $p_\mathrm{N} < 0$.

For small deformations the stiffness of the contact material can be described by a linear stress-strain curve with Young's modulus E of the contact material and the average normal stress σ_N. The normal strain ϵ_N can be approximated by the ratio of penetration p_N and total layer thickness L:

$$\sigma_\mathrm{N} = E\ \epsilon_\mathrm{N} = -E\ \frac{p_\mathrm{N}}{L} \ . \tag{2}$$

Using the average stress, the compression force F_c is calculated as a function of compression and material stiffness k_c:

$$F_\mathrm{c} = A\ \sigma_\mathrm{N} = -k_\mathrm{c1}\ p_\mathrm{N} \quad \text{with} \quad k_\mathrm{c1} = \frac{E\ A}{L} \ . \tag{3}$$

The stiffness of both colliding bodies, k_c1 and k_c2, are merged into a single collision stiffness k_c:

$$k_\mathrm{c} = \left(\frac{1}{k_\mathrm{c1}} + \frac{1}{k_\mathrm{c2}} \right)^{-1} \ . \tag{4}$$

Aside from the above description of the stiffness of the materials and the strain, it is also important to formulate the dynamic properties, i.e. elasticity of the collision. It is also referred to as coefficient restitution or bounciness of the collision [29]. The elasticity of a collision depends on the amount of dissipative energy lost during the impact. The most basic way is to model the contact surface as a visco-elastic Kelvin-Voigt material [30]. But, this model has several limitations, such as discontinuity of the contact force at the moment of impact, dependence of the coefficient of restitution on the mass of the impacting bodies and the lack

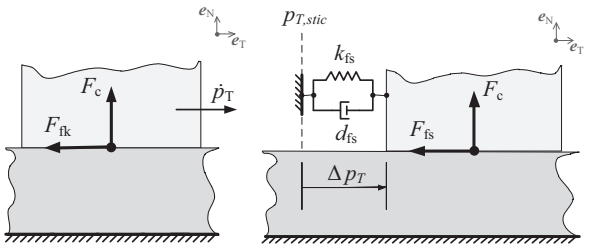

Fig. 3. Friction (a) and stiction (b) model.

of dependence on the impact velocity [29]. We therefore use the Hunt-Crossley model to extend (3) by a nonlinear damping component, which is comprised of the damping constant λ_c and the compression velocity $\dot{p}_N$, scaled by the penetration p_N [28]:

$$F_c = (\lambda_c\, p_N)\, \dot{p}_N - k_c\, p_N\ . \tag{5}$$

For the computation of the parameter λ_c, given certain prerequisites, please refer to [29]. An important property of the Hunt-Crossley model is that the contact forces are continuous upon impact, in contrast to the linear viscous damping model. Attracting forces ($F_c < 0$) only occur if the bodies are separated quickly by external forces. This can be interpreted such that the bodies lose contact because the relaxing speed of the compressed material is lower than the relative velocity of the bodies. For negative values of F_c, we therefore saturate $F_c = 0$:

$$\boldsymbol{F}_c = \begin{cases} \mathbf{0} & : \quad \dot{p}_N \geq \frac{k_c}{\lambda_c} \\ ((\lambda_c\, p_N)\, \dot{p}_N - k_c\, p_N) \cdot \boldsymbol{e}_N & : \quad \dot{p}_N < \frac{k_c}{\lambda_c} \end{cases} \tag{6}$$

2) Kinetic Friction: The direction of the friction force is the opposite of $\boldsymbol{e}_T$, which represents the direction of the relative contact velocity component perpendicular to the contact surface normal $\boldsymbol{e}_N$

$$\boldsymbol{e}_T = \frac{(\dot{\boldsymbol{p}} - (\dot{\boldsymbol{p}} \cdot \boldsymbol{e}_N) \cdot \boldsymbol{e}_N)}{\|(\dot{\boldsymbol{p}} - (\dot{\boldsymbol{p}} \cdot \boldsymbol{e}_N) \cdot \boldsymbol{e}_N)\|}\ . \tag{7}$$

The friction force in the tangential plane depends on the normal force, e. g., the collision force:

$$\boldsymbol{F}_{fk} = -\mu_{fk} \cdot F_c \cdot \boldsymbol{e}_T\ , \tag{8}$$

where μ_{fk} denotes the sliding friction coefficient, which depends on the materials of the colliding objects.

The friction force is directed opposite to the direction of the tangential velocity $\dot{p}_T$ (cf. Fig. 3(a)). If $\dot{p}_T$ is decreased below a minimum velocity v_{stic}, the kinematic friction changes to static friction.

3) Static Friction: Static friction is depicted in Fig. 3(b). The object sticks to the current position and reacts to external forces as a visco-elastic material. We assume the following Kelvin-Voigt model for the computation of the stiction force:

$$\boldsymbol{F}_{fs} = (-k_{fs} \cdot \Delta p_T - d_{fs} \cdot \dot{p}_T) \cdot \boldsymbol{e}_T \tag{9}$$

$$\text{with} \quad \Delta p_T = p_T - p_{T,stic}\ . \tag{10}$$

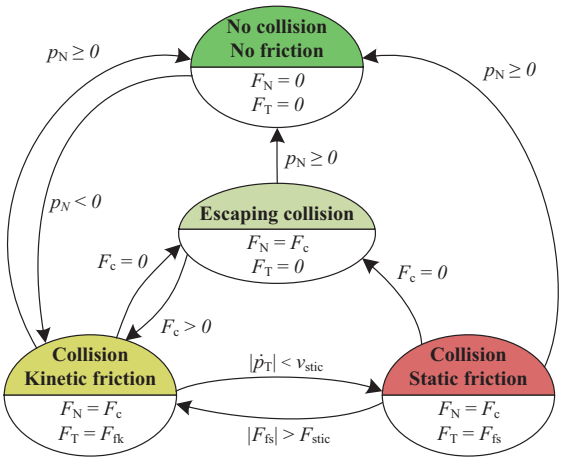

Fig. 4. State diagram of contact model.

$p_{T,stic}$ denotes the position at which the transition from friction to stiction occurs (cf. Fig. 3(b)). The transition to kinetic friction is triggered for static friction forces F_{fs} that exceed a defined maximum static friction F_{stic} which depends on the current normal force and the static friction coefficient μ_{fs} (cf. Fig. 4):

$$F_{stic} = \mu_{fs} \cdot F_c, \quad \mu_{fs} \geq \mu_{fk}\ . \tag{11}$$

Standard mechanics literature can be referred to for appropriate values of μ_{fs} and μ_{fk}. The values for k_{fs} and d_{fs}, however, are a bit more difficult to determine and require some tuning. Depending on the application and the material properties, usually a high stiffness is chosen for k_{fs} based on which d_{fs} is assigned an appropriate value.

4) Collision and Friction State Machine: Fig. 4 illustrates the computation process for modeling collisions, captured by the aforementioned equations, in form of states and triggering transition conditions.

5) Simulation Example: Simulation results of a bouncing contact of a metal object on a soft rubber surface are displayed in Fig. 5. The parameters used in the simulation example are listed in Table I. The elastic modulus $E = 0.01 \cdot 10^9\ \mathrm{N/m^2}$ for soft rubber is given in standard mechanics literature. With a thickness $L = 10\,\mathrm{cm}$ and a contact area of $A = 1\,\mathrm{cm}^2$, the resulting stiffness of the rubber layer is:

$$k_c = \frac{E \cdot A}{L} = 10^4\ \mathrm{N/m} \tag{12}$$

The elastic modulus of the metal object has no significant effect on the combined contact stiffness (cf. (4)).

6) Experimental Validation: We validated the presented contact model by comparing experimental measurements from a ball dropped on a force plate with the corresponding simulation results. Fig. 6 describes the experimental setup and results. The simulation results show a very good agreement with the ball motion and the contact forces at the first four bounces, later bounces in the experiment seem to be more damped. This is presumably due to energy dissipation at low velocities not considered in our model. Both peak values and shape of the highly transient contact situation

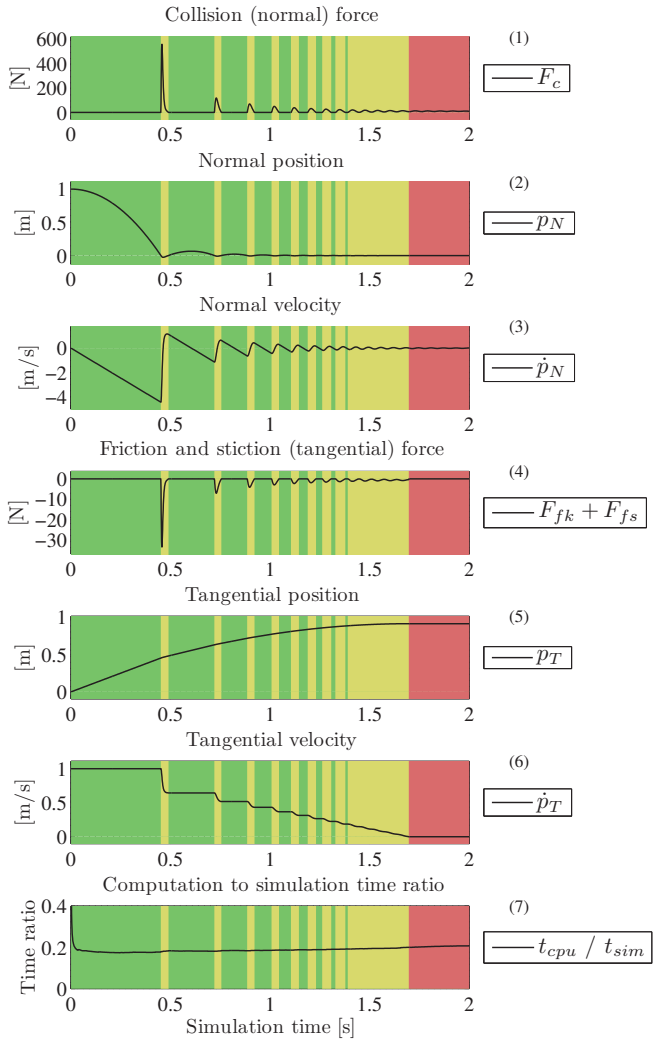

Fig. 5. Plot 1–3: no collision state (green), collision state (yellow, red), Plot 4–7: no collision state (green), kinetic friction state (yellow), static friction state (red). Solver settings: solver: [ode23 (bogacki-shampine)], relative tolerance: [$10^{(-3)}$], shape preservation: [enable all], number of consecutive minimum steps: [1], maximum simulation step width $\Delta t_{\max} = 1\,\text{ms}$; zero-crossing options: algorithm: [adaptive], number of consecutive zero crossings: [1000]; further available settings: [auto].

TABLE I

PARAMETERS USED IN THE SIMULATED COLLISION EXAMPLE

Parameter	Value	Parameter	Value
$p_{\text{N}}(0)$	1 m	μ_{fk}	0.06
$\dot{p}_{\text{T}}(0)$	1 m/s	μ_{fs}	0.1
m	1 kg	v_{stic}	0.001 m/s
k_{c}	10^4 N/m	k_{fs}	10^4 N/m
λ_{c}	$7.5 \cdot 10^3$ Ns/m^2	d_{fs}	40 Ns/m

forces are closely approximated by the simulation, as a close-up of one of the peak forces shows.

C. Modeling the Actuation

Following the constructed versions of BioRob arm and BioBiped, the actuation library includes models for a well established technology: rotary electric direct-current (DC)

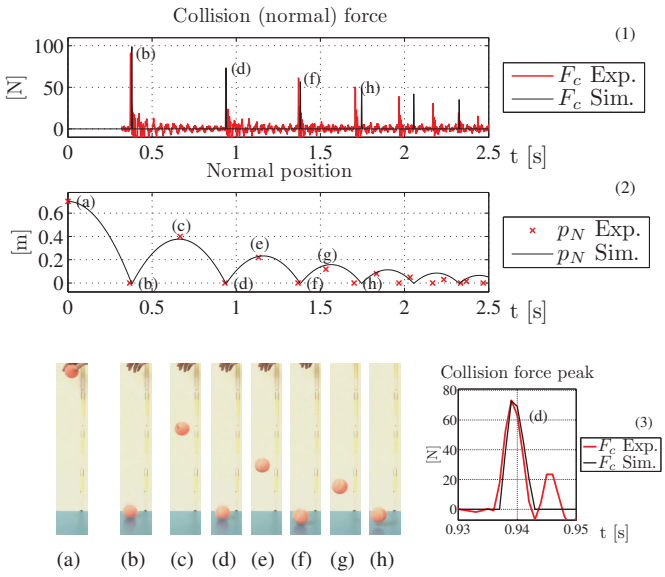

Fig. 6. Comparison of simulation and experimental data of a bouncing ball. A tennis ball is dropped on a force plate from a height of 70 cm. Plot (1) compares the simulated collision forces (black) with the measurements (red). Plot (3) displays a close-up from the second collision force peak. Pictures (a) to (h) come from the video recorded during the experiment and show the peak and collision positions of the ball. Plot (2) compares the ball positions read off the pictures with the simulation results. Simulation parameters: $m_{\text{Ball}} = 0.05\,\text{kg}$, $k_{\text{c}} = 1.7 \cdot 10^4\,\text{N/m}$, $\lambda_{\text{c}} = 2.4 \cdot 10^4\,\text{Ns/m}^2$, $p_{\text{N}}(0) = 0.7\,\text{m}$, $\dot{p}_{\text{N}}(0) = 0\,\text{m/s}$, $\dot{p}_{\text{T}}(0) = 0\,\text{m/s}$. The data of the force plate were measured with a rate of 1 kHz.

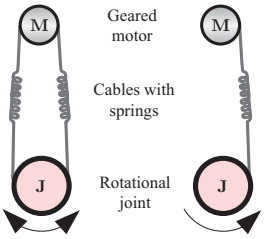

Fig. 7. Bidirectional versus unidirectional SEA.

motors with gears and mechanical springs. Both BioRob and BioBiped robots are driven by geared DC motors in conjunction with an elastic transmission that is coupled to a joint. The elastic transmission principle corresponds in its functionalities to that of the original Series Elastic Actuator (SEA) [31]. The advantages of series elastic actuation and the resulting low-impedance control have been elaborated in-depth: Storing energy and preventing damage due to shock represent only two reasons for this choice. Two slightly differing elastic transmission principles used in the BioRob and BioBiped robots are depicted in Fig. 7. The first is a so-called bidirectional SEA, where the gearbox is coupled by antagonistic cables with built-in extension springs to the joint. The second is a unidirectional SEA, where one of the cables is removed. More elaborate actuator models, including nonlinear transmission functions for the lever arms and nonlinear spring functions, are implemented as well. For equations of the bidirectional SEA please refer to [21].

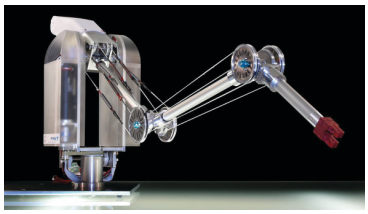

(a)

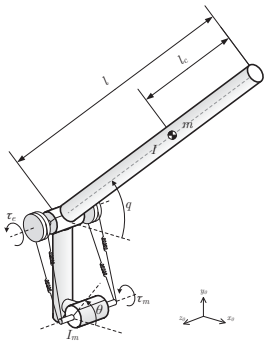

(b)

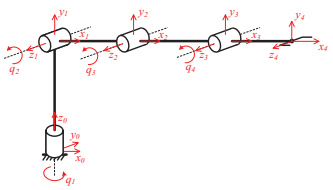

(c)

Link Lengths	
l_1	276 mm
l_2	307 mm
l_3	301 mm
l_4	80 mm

Link Masses	
m_1	2.00 kg
m_2	1.13 kg
m_3	0.53 kg
m_4	0.07 kg
total mass	3.73 kg

Fig. 8. From left to right: (a) BioRob-X4 robot; (b) abstraction of the actuation concept; (c) kinematic joint-link structure in zero position; table with link lengths and masses.

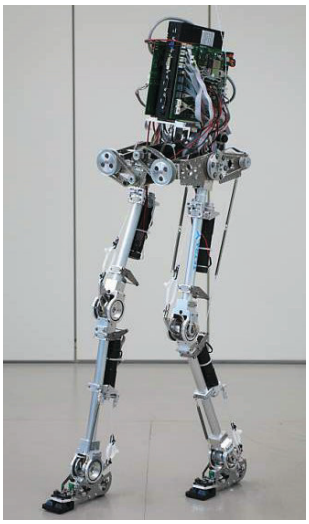

(a)

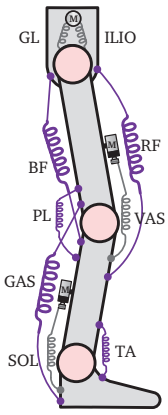

(b)

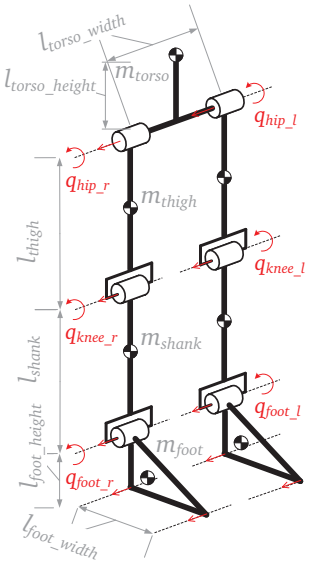

(c)

Link Lengths	
$l_{\mathrm{torso\_width}}$	150 mm
$l_{\mathrm{torso\_height}}$	270 mm
l_{thigh}	330 mm
l_{shank}	330 mm
$l_{\mathrm{foot\_height}}$	67 mm
$l_{\mathrm{foot\_width}}$	100 mm

Link Masses	
m_{torso}	4.7 kg
m_{thigh}	0.9 kg
m_{shank}	0.9 kg
m_{foot}	0.45 kg
total mass	9.2 kg

Fig. 9. From left to right: (a) BioBiped1 robot (photo: A. Karguth, TETRA GmbH); (b) abstraction of the actuation concept; (c) kinematic joint-link structure in zero position; table with link lengths and masses. The joint motion constraints of BioBiped1 correspond to those of humans: hip pitch $[-5°, 50°]$, knee pitch $[-90°, 0°]$ and ankle pitch $[-60°, 10°]$.

D. Controllers

Bio-inspired robots with high joint elasticities require specific controllers that take into account the complex dynamics in order to achieve the best possible performance. The implemented controllers range from classical PID controllers, that can track both joint and actuator reference signals considering saturation limits, to more sophisticated controllers with feedforward compensation and based on multijoint models that handle the effects of coupling among the joints.

E. Animation

An obvious goal of a MBS dynamics simulation is a realistic high-quality 3-D animation. SimMechanics visualization, while providing useful insight into the behavior of mechanical component, does not produce realistic animation and is not able to display the animation in real-time, especially when simulating with small time steps. Virtual Reality Toolbox, representing an interface between Matlab and Simulink data on one hand and virtual reality graphics on the other hand, can be used to achieve high-quality realistic animation. However, virtual reality graphics are based on VRML, an open standard for describing 3-D scenes. Depending on the background, the user may not be familiar with this standard and find it difficult to create a VRML file describing the 3-D scene to be visualized. Therefore, we created an animation tool based on OpenGL, that can also include general information such as time and trajectories (cf. Fig. 10 and 11).

III. APPLICATION TO REAL ROBOTS

Models and simulations of the manipulator and bipedal robot, BioRob and BioBiped, shown in Fig. 8(a) and Fig. 9(a), have been developed using the presented libraries.

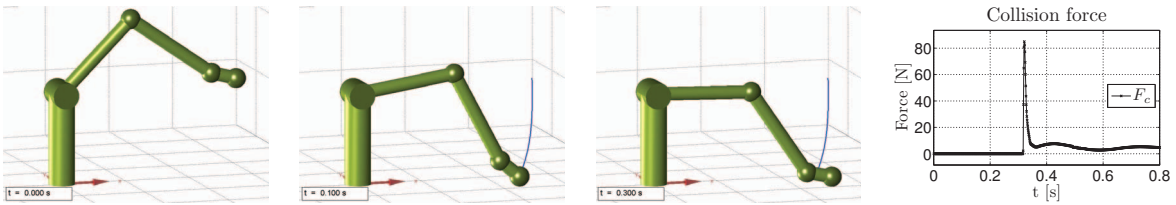

Fig. 10. BioRob arm colliding with the ground; normal collision forces at the end effector are depicted in the diagram on the right.

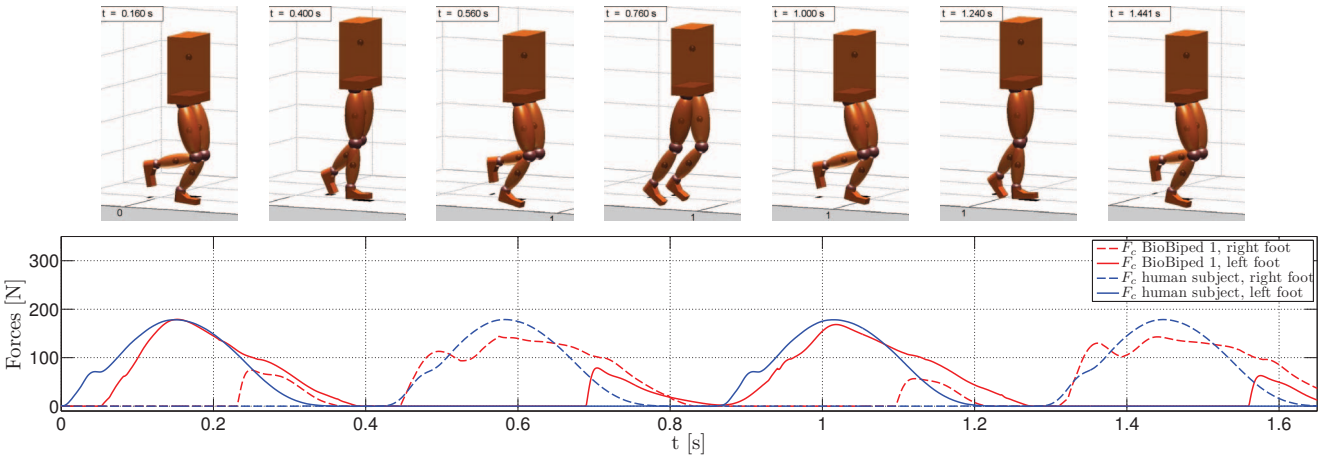

Fig. 11. Frames of the simulated BioBiped1 robot tracking a human-data based jogging motion with $\sim 2\,\mathrm{m/s}$. Simulated ground contact forces match the measured contact forces quite well.

This section describes how these complex structures have been modeled. Further, the behavior of the dynamic systems during contacts/collisions is demonstrated within two different scenarios.

A. Rigid joint-link structure and actuation

Both robots can be described on two levels containing, on the one hand, the kinematic rigid joint-link structure and, on the other hand, the actuation concept.

In Fig. 8(a) the BioRob arm is shown. It has four rotational degrees of freedom and consists of a lightweight structure weighing in total about 3.73 kg. Each joint is driven by a bidirectional SEA, as shown in Fig. 7. Cables with extension springs and pulleys elastically couple the geared DC motors to the joints. This actuation concept is depicted in Fig. 8(b). Its kinematic joint-link structure consisting of a base and four joint-link modules is displayed in Fig. 8(c). The table aside lists the link lengths and masses.

The BioBiped1 robot is shown in Fig. 9(a). It consists of a torso, which is modeled as a single body (cf. Fig. 9(c)), and two legs with two joints in the hip for the pitch and roll movement and one rotational joint each in knee and ankle for the pitch movement. Both legs are modeled as three joint-link serial chains and are attached to the torso, as illustrated in Fig. 9(c). Additionally, each leg is connected to one more link representing the foot sole. Links lengths and masses are given in the table of Fig. 9. As roll movements in the hip of real BioBiped1 robot are not yet considered, its modeling in the simulation has been so far omitted. The actuation concept differs from that of the BioRob arm (cf. Fig. 9(b)). Whereas the hip pitch joint is driven by a bidirectional SEA, both knee and ankle joints are actuated by a unidirectional SEA for the extension of the legs. The flexors in knee and ankle joint are only passively supported by serial elasticities. Further passive cables with extension springs take on the role of biarticular muscles, like in humans, to coordinate the synchronization of two leg joints. For further details regarding the actuation please refer to [23].

B. Contact blocks

Collisions are detected as soon as contact blocks, assigned to specific points of the rigid joint-link structures, are activated according to the computation process described in Section II-B. For this purpose, BioRob-X4 has a designated point contact at the end effector and BioBiped1 has designated point contacts at the heel and toe of each foot.

C. Application examples

The developed libraries and, particularly, the contact/collision model are tested in two application scenarios. Fig. 10 displays the BioRob arm colliding with the ground while it is tracking a preplanned trajectory. Slow jogging motions of BioBiped1 based on running joint angular data of a human subject [32] including the periodically occurring ground contacts are shown in Fig. 11. The simulated contact forces are compared to the measured contact forces of the human subject. Impressively, both the peak values and the typical single-humped patterns are matched quite well by the simulation results.

IV. CONCLUSIONS AND FUTURE WORKS

This paper briefly reviewed existing multibody simulation software packages and motivated the development of a new toolbox in Matlab/Simulink, tailored for general-purpose simulation of robotic arms and legs in direct contact with the environment. Distinctive features encompass ready-to-use rigid joint-link modules, which are extensible by compliant constraints and geared DC motor models including serial elasticities and pulley systems. Since paramount for a realistic simulation, special emphasis of this toolbox has been devoted to the modeling of realistic contact and impact forces. Tests with a bouncing ball indicated the plausibility of the proposed model and validated the forces computed in simulation. Further, we discussed the MBS dynamics models and simulation of BioRob-X4 and BioBiped1. The ground contact forces computed during a human-data based jogging motion of BioBiped1 agreed quite well with measured forces of a human subject. These results support the performed validation results all the more.

An important highlight of the simulation toolbox is its extensive use within two phd theses. Its utilization in the BioRob and BioBiped project allows for extensive testing. With continuing research and use of the toolbox, we expect to increase its maturity, thus, laying the foundations for its exposure to the robotics community. Publication of a further elaborated version of this simulation software may be helpful in advancing progress in robotics and easing the start for graduate students and novices at robotics. To enhance its usability for a large number of research projects, we will extend the contact model to detect more complex geometrical contacts. Besides, we will enhance the flexibility and user-friendliness of the developed animation methods. These extensions and additions will increase the maturity of the libraries and the compatibility to the well-known and often used Robotics toolbox. Other future directions include, but are not limited to, developing interfaces to other environments such as Mathematica in order to enable the synchronization of equations of motion with the models developed using our toolbox.

REFERENCES

[1] J. Craig, *Introduction to Robotics Mechanics and Control*. Addison-Wesley Pub. Co., 1989.

[2] R. Featherstone, *Robot Dynamics Algorithms*. Kluwer, 1987.

[3] T. Kane, *Dynamics: Theory and Applications*. McGraw-Hill, 1985.

[4] H. Goldstein, *Classical Mechanics*. Addison-Wesley Pub. Co., 1980.

[5] D. K. Pai, U. M. Ascher, and P. G. Kry, "Forward dynamic algorithms for multibody chains and contact," in *IEEE International Conference on Robotics and Automation*, 2000.

[6] M. W.Walker and D. E. Orin, "Efficient dynamic computer simulation of robotic mechanisms," *Journal of Dynamic Systems, Measurement, and Control*, vol. 104, pp. 205–211, 1982.

[7] K. Yamane and Y. Nakamura, "Dynamics simulation of humanoid robots: Forward dynamics, contact, and experiments," in *17th CISM-IFToMM Symposium on Robot Design, Dynamics, and Control*, 2008.

[8] R. Featherstone and D. E. Orin, *Handbook of Robotics*. Springer, 2008, ch. Dynamics, pp. 35 – 65.

[9] R. L. Smith, *Open Dynamics Engine v0.5 User Guide*, http://www.ode.org/, 2006.

[10] J. Denavit and R. S. Hartenberg, "A kinematic notation for a lower-pair mechanisms based on matrices," *ASME Journal o Applied Mechanics*, vol. 22, pp. 215–221, 1955.

[11] P. Corke, "A robotics toolbox for matlab," *IEEE Robotics and Automation Magazine*, pp. 24–32, 1996.

[12] J. F. Nethery and M. W. Spong, "Robotica: A mathematica package for robot analysis," *IEEE Robotics and Automation Magazine*, pp. 13–20, 1994.

[13] P. U. Lee, D. C. Ruspini, and O. Khatib, "Dynamic simulation of interactive robotic environment," in *IEEE International Conference on Robotics and Automation*, 1994, pp. 1147–1152.

[14] D. C. Ruspini and O. Khatib, "Collision/contact models for the dynamic simulation of complex environments," in *International Symposium on Robotics Research*, 1997, pp. 185–195.

[15] D. Ruspini and O. Khatib, "A framework for multi-contact multi-body dynamic simulation and haptic display," in *IEEE/RSJ International Conference on Intelligent Robots and Systems*, vol. 2, 2000, pp. 1322–1327.

[16] L. Zlajpah, "Integrated environment for modelling, simulation and control design for robotic manipulators," *Journal of Intelligent and Robotic Systems*, vol. 32, pp. 219–234, 2001.

[17] D. N. Vila-Rosado and J. A. Dominguez-Lopez, "A matlab toolbox for robotic manipulators," in *6th Mexican Int. Conf. on Computer Science*, 2005.

[18] B. Nguyen and J. Trinkle, "Modeling non-convex configuration space using linear complementarity problems," in *IEEE International Conference on Robotics and Automation*, 2010, pp. 2316–2321.

[19] E. Todorov, "Implicit nonlinear complementarity: A new approach to contact dynamics," in *IEEE International Conference on Robotics and Automation*, 2010, pp. 2322–2329.

[20] Biorobassist project website. [Online]. Available: www.biorobassist.de

[21] T. Lens, J. Kunz, and O. von Stryk, "Dynamic modeling of the 4 dof biorob series elastic robot arm for simulation and control," in *Simulation, Modeling, and Programming for Autonomous Robots (SIMPAR 2010)*, ser. Lecture Notes in Artificial Intelligence. Springer, 2010, pp. 411–422.

[22] Biobiped project website. [Online]. Available: www.biobiped.de

[23] K. Radkhah, C. Maufroy, M. Maus, D. Scholz, A. Seyfarth, and O. von Stryk, "Concept and design of the BioBiped1 robot for human-like walking and running," *Special Issue on "Advances on Humanoid Robot Body-ware Design and Development" in International Journal of Humanoid Robotics*, 2011, conditionally accepted.

[24] *Matlab User's Guide*, The MathWorks, Inc., Natick, MA, 1990.

[25] *Simulink User's Guide*, The MathWorks, Inc., Natick, MA, March 2007.

[26] K. Yamane and Y. Nakamura, "Dynamics filter – concept and implementation of online motion generator for human figures," *IEEE Transactions on Robotics and Automation*, vol. 19, no. 3, pp. 421–432, 2003.

[27] Y.-T. Wang, V. Kumar, and J. Abel, "Dynamics of rigid bodies undergoing multiple frictional contacts," in *Robotics and Automation, 1992. Proceedings., 1992 IEEE International Conference on*, May 1992, pp. 2764 –2769 vol.3.

[28] K. H. Hunt and F. R. E. Crossley, "Coefficient of restitution interpreted as damping in vibroimpact," *Journal of Applied Mechanics*, vol. 42, no. 2, pp. 440–445, 1975.

[29] D. Marhefka and D. Orin, "Simulation of contact using a nonlinear damping model," in *Robotics and Automation, 1996. Proceedings., 1996 IEEE International Conference on*, vol. 2, Apr. 1996, pp. 1662 –1668 vol.2.

[30] W. Goldsmith, *Impact: The theory and physical behaviour of colliding solids*. Dover Publications, 2001.

[31] G. A. Pratt and M. M. Williamson, "Series elastic actuators," in *IEEE International Workshop on Intelligent Robots and Systems*, 1995, pp. 399–406.

[32] S. Lipfert, "Kinematic and dynamic similarities between walking and running," Ph.D. dissertation, Friedrich-Schiller-Universität, Jena, Germany, 2009.